

General Disclaimer

One or more of the Following Statements may affect this Document

- This document has been reproduced from the best copy furnished by the organizational source. It is being released in the interest of making available as much information as possible.
- This document may contain data, which exceeds the sheet parameters. It was furnished in this condition by the organizational source and is the best copy available.
- This document may contain tone-on-tone or color graphs, charts and/or pictures, which have been reproduced in black and white.
- This document is paginated as submitted by the original source.
- Portions of this document are not fully legible due to the historical nature of some of the material. However, it is the best reproduction available from the original submission.

Test Results of a Ten Cell Bipolar Nickel-Hydrogen Battery

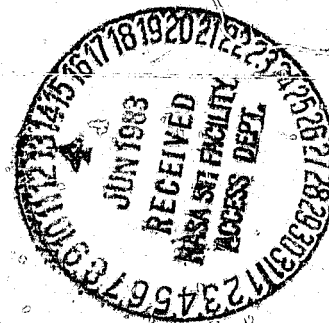
(NASA-TM-83384) TEST RESULTS OF A TEN CELL
BIPOLAR NICKEL-HYDROGEN BATTERY (NASA) 11 p
HC A02/MF A01 CSCL 10C

N83-26253

Unclas
03832

G3/44

Robert L. Cataldo
Lewis Research Center
Cleveland, Ohio



Prepared for the
Eighteenth Intersociety Energy Conversion Engineering Conference
cosponsored by the AIChE, IEEE, AIAA, ACS, ANS, ASME, and SAE
Orlando, Florida, August 21-26, 1983

NASA

TEST RESULTS OF A TEN CELL BIPOLAR NICKEL-HYDROGEN BATTERY

Robert L. Cataldo

National Aeronautics and Space Administration
Lewis Research Center
Cleveland, Ohio 44135

INTRODUCTION

Space power systems of the future are projected to require power levels that extend far beyond those currently in the 1 kW range. High power systems will most likely utilize either higher battery voltages in the 200V-300V range or special power processing equipment to convert low battery voltage to high system voltage. This second option will demand batteries with high capacity (greater ampere-hours per cell or cells configured in parallel), and high discharge current capability. The energy storage for such large systems becomes a challenging battery engineering problem.

The two candidate battery systems for space power are nickel-cadmium and nickel-hydrogen. Presently, both these types are available in capacities ranging from 30 to 50 ampere-hours. The energy storage for a low-earth orbit mission requiring 35 kW of power would contain about 500 individual 50 ampere-hour cells, arranged in series and/or parallel. No battery of this magnitude has yet been constructed and tested, and there are serious concerns about the feasibility of such a system for the long lifetimes required in low earth orbit.

In light of this problem, a study was initiated in late spring of 1981 at the NASA Lewis Research Center to design and evaluate a new design concept for nickel-hydrogen cells. This concept involved constructing a battery in a bipolar stack with cells consisting of one plate for each nickel and hydrogen electrode. Preliminary designs at the system level of this concept promised improvements in both volumetric and gravimetric energy densities, thermal management, life extension, costs and peak power capability over more conventional designs. (1)

To get an early confirmation of these encouraging design studies, a concept verification program was initiated. The first phase of the program was the design and assembly of a preprototype bipolar battery. The design incorporated hardware and components available from past programs along with some that were specially constructed. The size of the cell hardware (10 cm x 21 cm active area) allowed the use of a 6.5 ampere-hour capacity nickel electrode. Ten of these cells were assembled into a stack with the dimensions length - 35.4 cm, height - 15.2 cm,

width - 10 cm. The second phase included a series of characterization and cycle tests.

The following discussion of oxygen, electrolyte and thermal management, convey the design philosophies incorporated into the bipolar concept as applied to nickel-hydrogen batteries. Use of these concepts offers a high probability of a successful design which theoretically would yield good performance and long life.

OXYGEN MANAGEMENT

In prior designs, oxygen generated on overcharge has been allowed to combine with hydrogen at the hydrogen electrode. A separate electrode for recombination would prevent damage to the hydrogen electrode from the heat generated. The approach taken in this design was to have recombination occur behind the Ni electrode (1). Figure 1 depicts the methodology used. A high bubble pressure asbestos separator forces the O₂ into a highly porous electrolyte reservoir plate. The recombination sites are strips of hydrogen electrodes 0.47 cm x 19 cm. They are encapsulated in a vapor permeable tubing to allow passage of gases in, and water vapor out. The tubing also isolates the catalyst electrically, preventing parasitic reaction between the recombination sites and the nickel electrode. This method of oxygen management also benefits the overall electrolyte management scheme by keeping the recombined water from possibly flooding the hydrogen electrode.

ELECTROLYTE MANAGEMENT

Electrolyte management can have a significant effect on the cycle life of a nickel-hydrogen battery and should be a prime consideration of the overall battery design. The objective of electrolyte management is to prevent flooding of the hydrogen electrodes and drying of the nickel electrodes and separators. The approach taken to achieve this objective is through pore size selection of components such that each component has the optimum amount of electrolyte (2).

The electrolyte reservoir plate has a pore size that freely accommodates the water formed during the charge portion of the cycle and returns electrolyte by wicking to the nickel electrode and separator as required. The wicking action is created by choosing a reservoir plate with larger

pores than the electrode and separator and maintaining physical contact. Flooding of the hydrogen electrode is also prevented by proper pore size selection as well as use of hydrophobic materials in the electrode.

THERMAL MANAGEMENT

In the present design heat is primarily rejected from the stack by cooling fins which are that part of the bipolar plates that extend beyond the frame edges. Thus, the heat generated during cycling is transferred by a combination of conduction and convection to the test chamber wall. Cell temperatures did not exceed 29°C (84°F) at the end of discharge. Therefore, this method of cooling is adequate at the power levels being tested. However, larger power levels would require alternate heat rejection options such as heat pipes or cooling plates within the stack with gaseous or liquid recirculating coolant.

CELL COMPONENTS

The following paragraphs describe the composition, manufacture, and function of the components used in the cell.

GAS FLOW SCREEN

The flow screen for the hydrogen electrode was expanded nickel of 1.05 mm (0.042 in.) thickness with approximately 95% open area.

NICKEL ELECTRODE

The nickel electrodes used in the battery are chemically impregnated, pressed powder sinter type electrodes remaining from a previous program. These electrodes have a screen grid and an average loading of 2.1 grams/cc of void volume. The electrodes for this application were cut slightly smaller than the frame dimensions to allow for electrode expansion. The electrode thicknesses ranged from 0.96 mm to 1.0 mm. The capacity of the electrode was calculated to be about 6.50 ampere hours with a surface area of 218 cm² (one side).

HYDROGEN ELECTRODE

The hydrogen electrode was a fuel cell type catalyzed porous screen electrode. Electrode dimensions were: 0.025 cm thick, 10.1 cm wide, and 21.6 cm long, with a surface area of 218 cm² (one side). Other electrode properties are proprietary to the manufacturer.

SEPARATOR

The separator material was a beater treated asbestos (BTA). BTA is a reconstituted blend of asbestos sheets with a 5% latex binder. The experimentally determined bubble pressure (pressure at which the first bubble passes through the separator) is 2.0 atmospheres. The dimensions of the separator are 11.9 cm wide by 23.3 cm long making it larger than the

electrodes. This extra separator area, along with six wick rings, forms a seal with the frame ledge to provide a barrier against oxygen passage to the hydrogen electrode (Figure 2). The uncompressed thickness of the separator is 0.053 cm (21 mils), while the average compressed thickness is designed to be 0.025 cm (10 mils).

ELECTROLYTE RESERVOIR PLATE

The electrolyte reservoir plate (ERP) was a foam nickel structure with a density of 10%. Each plate was compressed from 0.25 cm to 0.125 cm, followed by cutting with a rule die that cut out four slots 0.8 cm wide and 20.6 cm long to house the recombination strips. The average pore diameter is 0.025 cm (10 mils). This pore size allows the passage of hydrogen and oxygen gas through the ERP to the recombination sites. The water that is formed at the recombination sites during charge and overcharge is freely wicked out of the ERP by the separator and nickel electrode since these cell components have smaller pores.

BATTERY HARDWARE

The hardware used for the bipolar battery was originally a carbon dioxide removal unit for the life support system on the Apollo missions. The configuration of the unit was such that it could readily be utilized for verification testing of a bipolar nickel-hydrogen battery. The items used from the unit were ten polysulfone frames, eleven gold-plated nickel bipolar plates, two polysulfone insulation plates, and two stainless steel end plates.

The injection molded polysulfone frames were used to contain the cell components and electrolyte. The nominal frame thickness was 0.378 cm (.149 in) as shown in Figure 2. The inner frame ledge provides a means of sealing the separator around the nickel electrode, thus eliminating evolved oxygen passage to the hydrogen electrode. Hydrogen gas was channeled to the hydrogen electrode via slots connecting the inner frame to two manifolds. The 16 slots provide 0.515 cm² of area for hydrogen gas ingress/egress. These slots were in line with the gas flow screen (expanded nickel). Similar slots and manifolding were provided on the other side of the frame to supply hydrogen gas to the recombination sites. The total slot area for this side was 0.296 cm² and these slots align with the electrolyte reservoir plate.

The bipolar plates are thin gold-plate nickel sheets and were sandwiched between each frame. Each cell was enclosed between two bipolar plates. A neoprene gasket fit into a recess in the frame and seals against the bipolar plate, retaining the electrolyte within each cell. External current connections were made to the bipolar plates on each end. The interior bipolar plates conduct current from the positive electrode of one cell to the negative electrode of the next, thus no intercell electrical connectors were needed. However, electrical connections were made to each plate to monitor

ORIGINAL PAGE IS OF POOR QUALITY

individual cell voltages. The bipolar plate was also used for heat rejection. Each plate extends beyond the frame on two opposite sides forming a set of cooling fins.

The stainless steel end plates and tie bolts compressed the cell components and gaskets. The cell compression was designed for a nominal 0.028 cm (.011 in), which compressed the separator from 0.053 cm to 0.025 cm. The manifolds formed by the cell frames and end plates allowed for vacuum electrolyte fill and drain.

Life Systems Inc. of Beechwood, Ohio has loaned to NASA Lewis Research Center the following hardware: cell frames, stack end plates, insulation plates, tie bolts, and bipolar plates to help expedite the verification testing of the bipolar concept as applied to nickel-hydrogen batteries.

STACK ASSEMBLY

The following sequence was used to assemble the stack components:

1. The negative side end plate was placed in position.
2. the negative side insulation plate and "O" rings were positioned.
3. Six guide pins were inserted into bolt holes for alignment of subsequent parts.
4. The negative terminal bipolar plate was positioned.
5. The hydrogen side gasket was placed over the guide pins.
6. The polysulfone frame was positioned on the gasket.
7. The cell components were inserted in the frame cavity in the following order:
 - a) hydrogen flow screen
 - b) hydrogen electrode
 - c) separator
 - d) nickel electrode
 - e) wick rings
 - f) electrolyte reservoir plate
 - g) recombination strips
8. The nickel side gasket was lowered over the guide pins.
9. The bipolar plate was positioned on the gasket.

Steps 5-9 were repeated for the next nine cells followed by the positive side insulation plate and end plate. The tie bolts were inserted from the negative side and threaded into the positive side end plate with 3 inch-pounds of torque.

The stack was then placed in a hydraulic press with an applied force of 5000 pounds. The tie

bolts were retorqued to 10 inch-pounds. The press was readjusted to 5000 pounds and the tie bolts were torqued to 15 inch-pounds. This step was repeated once more.

ELECTROLYTE FILL AND DRAIN

Two acrylic plates were fitted to the stack end plates with gaskets and C-clamps. The acrylic plates had tube fittings adjacent to the manifold openings. After a vacuum was pulled on the stack, a 31% potassium hydroxide solution was valved into the stack. The stack remained filled over night and was then drained of excess electrolyte over a period of several hours. The manifolds were then wiped clean of excess electrolyte and the stack inserted into the test chamber. The test chamber was evaluated, leak checked and filled with hydrogen at 50 PSI. (The test chamber was an oversize pressure vessel and the pressure changes during cycling were negligible.)

TEST PROCEDURES

Initial testing was carried out in several phases. First, characterization tests were run to determine the performance of the bipolar nickel-hydrogen battery. Following the successful completion of this test matrix, the second phase of tests was initiated. Low-earth orbit (LEO) cycle tests were run with a depth-of-discharge of 80%. The third phase was to determine the peak power capability of the battery.

The characterization tests were carried out at three charge levels, C/4, C/2 and C rate. The capacity of the battery is designated as 6.5 ampere-hours based on a C/4. Discharge rates (constant current) used in the characterization matrix were C/4, C/2, C and 2C. The recharge ampere-hours were the same (6.5 Ahr) for all conditions of the test matrix regardless of discharge rate. Therefore, the battery received an overcharge at conditions where discharge rates were high. The discharge was terminated when the voltage of the weakest cell in the stack fell to 0.5V.

LEO cycling tests were run at one hour charge and half-hour discharge intervals. (The battery was rated at 6.0 Ahr for the LEO testing, based on the 1.6C discharge rate to be used in this testing.) Constant current charge and discharge rates were employed for this phase of testing. The depth of discharge was set at 80%, giving a discharge current of 9.6 amperes. A recharge fraction of 1.10 of the rated capacity was necessary for end of discharge voltage stabilization. A peak power test was carried out at the end of 100 LEO cycles. Using a programmable load the discharge current was increased until the power passed its maximum value.

After completion of the peak power tests, the test chamber was opened and the stack examined. Cell number one was removed from the stack solely

for evaluation and analysis (no anomalies were evident in the data). This also would permit possible problem areas within the cell or stack to be discovered at an early date. The stack was then reassembled with nine cells and placed on LEO cycling tests to establish an operational data base.

INSTRUMENTATION

The individual cell voltages and the stack current were monitored and recorded. Cell temperatures were monitored but not recorded. Temperatures were measured on the fin of the bipolar plate with an iron-constant thermocouple. Computer-generated data includes ampere-hours and watt-hours with integration intervals of every 18 seconds.

RESULTS

Characterization test results are shown in Figures 3 and 4. Figure 3 shows ampere-hour and watt-hour efficiencies at different charge and discharge levels. The equations used to determine efficiencies are:

$$\frac{I_d \times T_d}{I_c \times T_c} \times 100 = \text{ampere hour eff.}$$

$$\frac{P_d \times T_d}{P_c \times T_c} \times 100 = \text{watt-hour eff.}$$

where: I = current (amps) c = charge
P = power (watts) d = discharge
T = time (hrs)

In general, the efficiencies increased as the charge rate is increased, which is consistent with nickel electrode behavior in other battery systems such as nickel-cadmium and nickel-zinc. Figure 3 further shows that efficiencies increase as the discharge rate decreases. This is expected; however, since a fixed recharge of 6.5 ampere-hours was returned each test, the highest rate discharges were penalized by being overcharged. Figure 4 shows a family of curves at the different discharge rates. An additional curve was added for the 10C (65 amperes) discharge rate. This data was obtained when the discharge equipment malfunctioned during LEO cycling. Five ampere-hours were withdrawn (83% DOD) in just under six minutes.

A LEO cycle regime of 60 min. charge, 30 min. discharge, 80% DOD with 1.10 recharge fraction would correspond to a 1.6C rate discharge and a 1.10 C rate charge and would be predicted to have amp-hour and watt-hour efficiencies of about 88 and 76 percent, respectively.

The peak power was determined following the 100th LEO cycle. The battery current and voltage was 165 amperes (about 27C) and 6.6 volts, respectively, supplying 1.1 kW of power. This is shown in Figure 5. The peak power

would probably have been higher but the power leads were only two #14 AWG wires connecting the stack to the terminals that were mounted in the vessel. In addition, the slip-on type electrical connectors that attach to the end plates are rated for about 10 amperes. These factors contribute to a significant voltage drop.

Following the peak power test, one end cell was removed for evaluation and the physical appearance of the stack observed. The nickel electrode was measured for growth. A 10% increase in thickness and a 2-3% increase in length and width were noted. The hydrogen electrode appeared as that of an unused electrode. The separator was wet and could be easily separated from the electrodes intact. The ERP was damp but not wet with electrolyte. The strips of hydrogen electrode used for recombination showed no evidence of burning.

Some evidence of corrosion was noted on the positive end bipolar plate inside the manifold. The substance was analyzed and found to be a nickel compound. Its greenish color suggests the substance was probably nickel carbonate or nickel nitrate. An electrolyte film probably remained on the inner surface of the manifold, even after a thorough cleaning, which most likely contributed to the corrosive actions. The bottom of the vessel was damp with electrolyte. Several causes were postulated; these being insufficient draining time, electrolyte forced out during vessel evacuation preceding the hydrogen fill or electrolyte forced out during charge. If the electrolyte was due to the latter cause, it would have only occurred during the early cycles, since such a process continuing over 2000 cycles would tend to cause resistive cells (high polarization voltage) which had not been observed.

The stack was refilled with electrolyte and drained. The nine-cell stack was again placed on LEO cycle testing. Initially a minimum end-of-discharge voltage of 1.20 V per cell was obtained with a 1.10 recharge fraction, a charge of 5.3 ampere-hours and a 4.8 ampere-hour discharge. After 600 cycles, cell #4 would reach 0.50 volts prematurely, terminating the half-hour timed discharge. The battery was then deep-discharge reconditioned by placing a 10 ohm resistor across the terminals, followed by a short circuit overnight. The battery was then charged for two hours at a current of 6.5 amperes and placed on cycle test with a recharge fraction of 1.20. After 182 additional cycles, cells 3, 4, and 5 exhibited voltages in the 0.80 volt range at the end-of-discharge. Shunt currents were suspected, therefore the stack was removed from the pressure tank and wiped clean. Evidence of free electrolyte was found in the manifolds and a few drops between the bipolar plate fin area. When the stack was replaced into the test chamber more electrolyte came out. The stack was then cleaned in place.

After another 200 cycles at a recharge fraction of 1.20 cell #3 again had a low end-of-discharge voltage. After a complete charge, cell #3 was

charged individually through the voltage data leads with an additional 3 ampere-hours. After 4 cycles cell #3 had low voltage again. The whole stack was then deep-discharge reconditioned in the same manner as before. All weak cells recovered, maintaining 1.20 volts per cell after the half-hour discharge. The recharge fraction was varied over three levels, 1.20, 1.15, and 1.10. Figure 6 shows that a recharge fraction of 1.10 cannot maintain 1.2 volts per cell at end-of-discharge. Shunt currents formed by electrolyte paths between cells could be the cause for the need to increase the recharge fraction.

An open circuit self-discharge test was conducted to determine if any shunt currents existed. Figure 7 shows individual cell voltages on open circuit. Cell #3 went to zero volts after 53 hours. This corresponds to about a 120 milliamperes average shunt current. Cells #4 and #5 also possess shunt currents, but of a lesser magnitude. The other cells have a normal self-discharge curve. Electrolyte bridges will divert a portion of the charge current, thus contributing to the need for larger recharge fractions when shunt currents are present. However, the battery is still operable, but at reduced efficiency.

Constant voltage charging was tested to provide some additional operational data, since many spacecraft use this mode of charging. Figure 8 shows a charge/discharge voltage profile of an early cycle. Original indications were that constant voltage charge method was a more efficient method, because charge voltages were lower than constant current voltages. However, over a few days of increasing the charge voltage to stabilize end-of-discharge voltage, a recharge fraction of 1.30 could not maintain a 1.2 volt end of discharge voltage.

CONCLUSIONS

Test results of the first NASA Lewis Research Center bipolar nickel-hydrogen battery are most encouraging. This preprototype battery, built with less than ideal components and hardware, exceeded expectations. A total of 2000 LEO cycles at 80 percent depth of discharge have been accrued. A cycle life goal of 30,000 cycles appears achievable with minor design changes. These improvements include advanced technology nickel electrodes, insulated bipolar plates and specifically designed frames to minimize shunt currents.

The discharge rate capability of this design exceeds 25C. At the 10C discharge rate, 80% of the battery capacity can be withdrawn in six minutes. This data shows that the bipolar design is well suited for those applications requiring high peak power pulses.

Deep discharge reconditioning improved end-of-discharge voltages on LEO cycling, while overcharge techniques were much less effective. Those cells with probable shunt currents had

improved capacity performance following reconditioning.

Low polarization voltages, which result in a cyclic watt-hour efficiency of 76-80%, have been demonstrated, an improvement over other more conventional nickel-hydrogen designs. This will result in reduced weight of the solar array and power processing components. Additional weight savings are realized with the battery itself. Thus the high voltage bipolar stack within one common pressure vessel makes an ideal building block for large advanced energy storage systems for applications like the manned space station.

REFERENCES

1. Cataldo, R. L. and J. J. Smithrick, "Design of a 35-Kilowatt Bipolar Nickel-Hydrogen Battery for Low-Earth-Orbit Applications," in 17th IECEC Proceedings, Vol. 2, pp. 780-783, IEEE, New York (1982).
2. Abbey, K. M. and L. H. Thaller, "Pore Size Engineering Applied to Starved Electrochemical Cells and Batteries," in 17th IECEC Proceedings, Vol. 2, pp. 757-764, IEEE, New York (1982).

ORIGINAL PAGE IS
OF POOR QUALITY

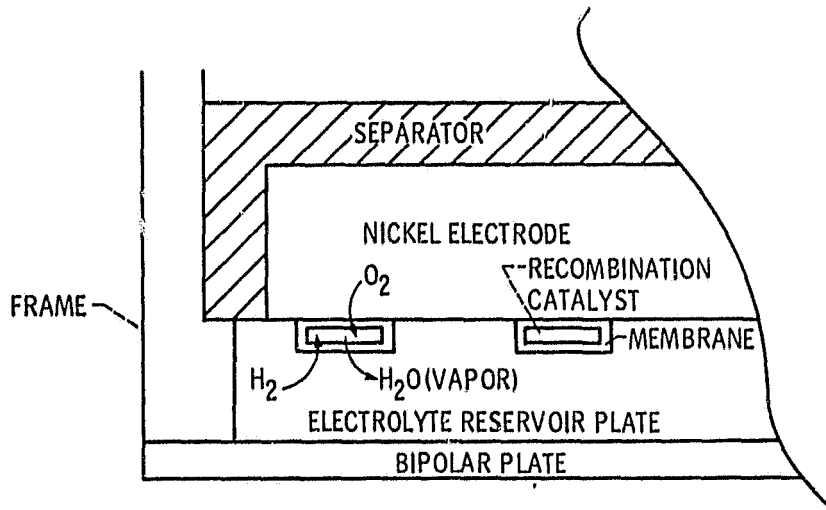


Figure 1. - Graphic representation of oxygen - hydrogen recombination.

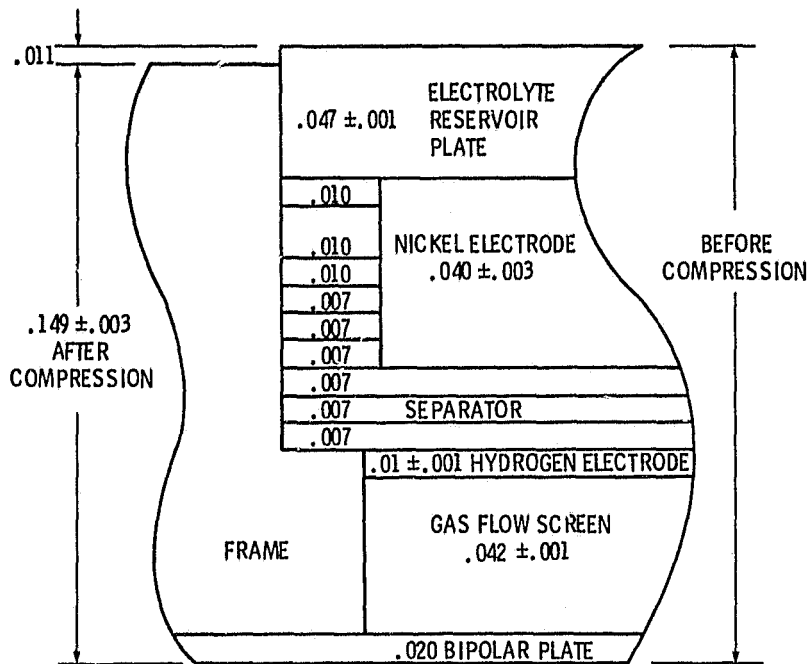


Figure 2. - Cell cross section with dimensions of components, in.

ORIGINAL PAGE IS
OF POOR QUALITY

DISCHARGE RATE	C/4		C/2		C	
	A-H	W-H	A-H	W-H	A-H	W-H
C/4	93.7	86	97	88	98.3	88
C/2	88.6	81	87	78	93	82
C	88	78	91	80	88	76
2C	86	73	90	76	90	75

Figure 3. - Ampere hour and watt hour efficiencies at various charge and discharge rates.

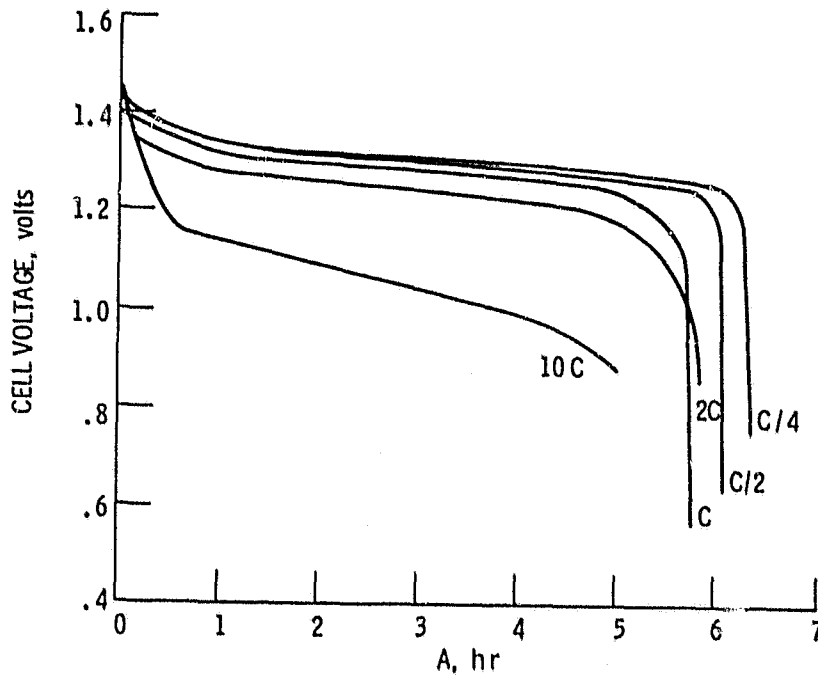


Figure 4. - Discharge voltage vs ampere hours out at the C/4, C/2, C, 2C and 10C rate.

ORIGINAL PAGE IS
OF POOR QUALITY

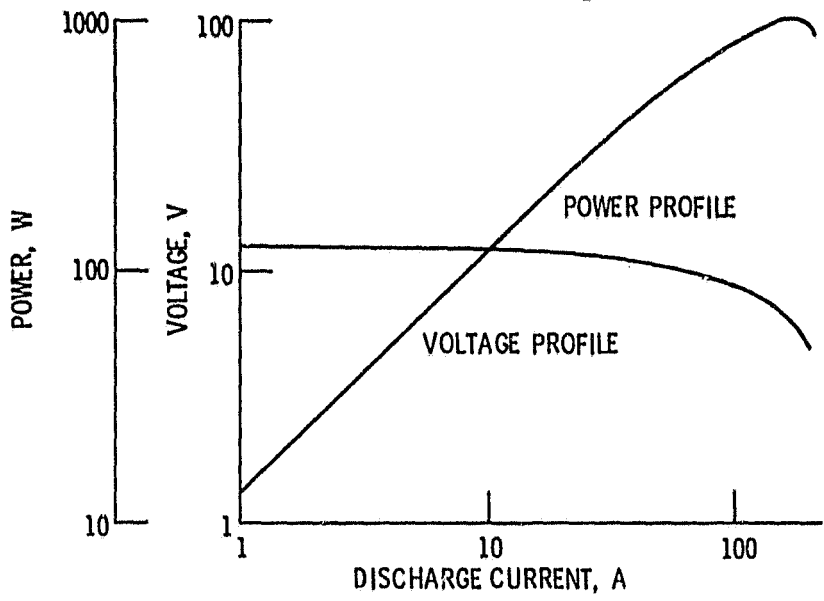


Figure 5. Voltage and power profiles for increasingly ramped discharge current.

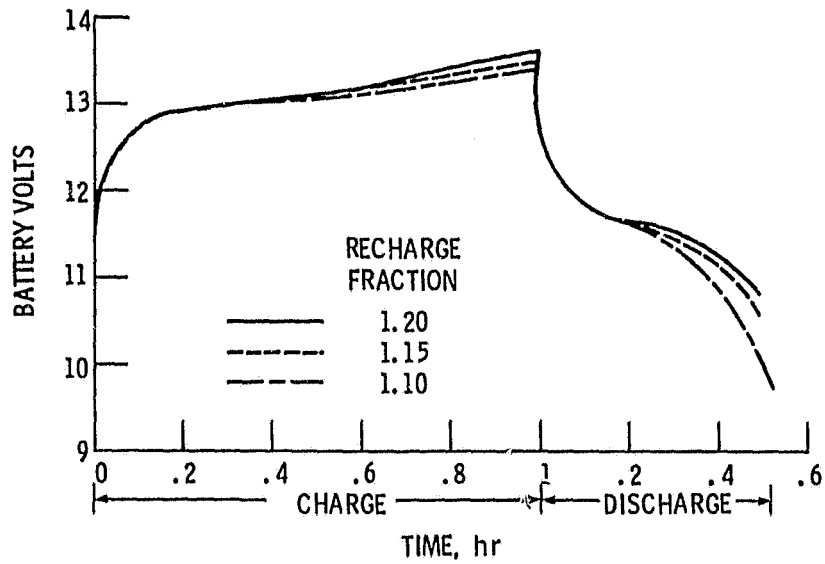


Figure 6. - Cyclic battery voltage for recharge fractions of 1.20, 1.15 and 1.10.

ORIGINAL PAGE IS
OF POOR QUALITY

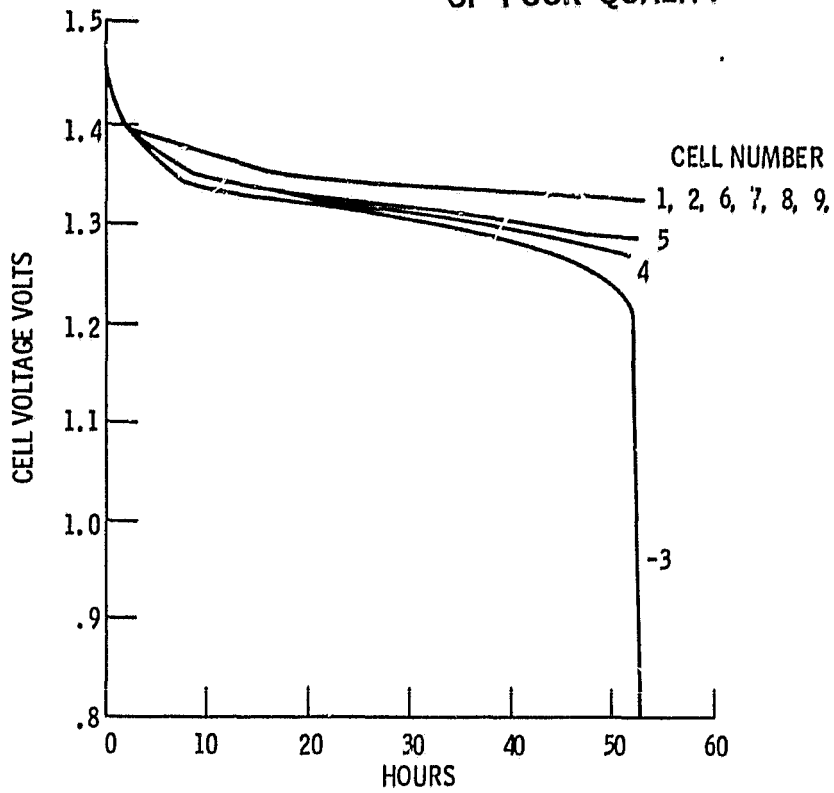


Figure 7. - Individual cell voltages on open circuit stand.

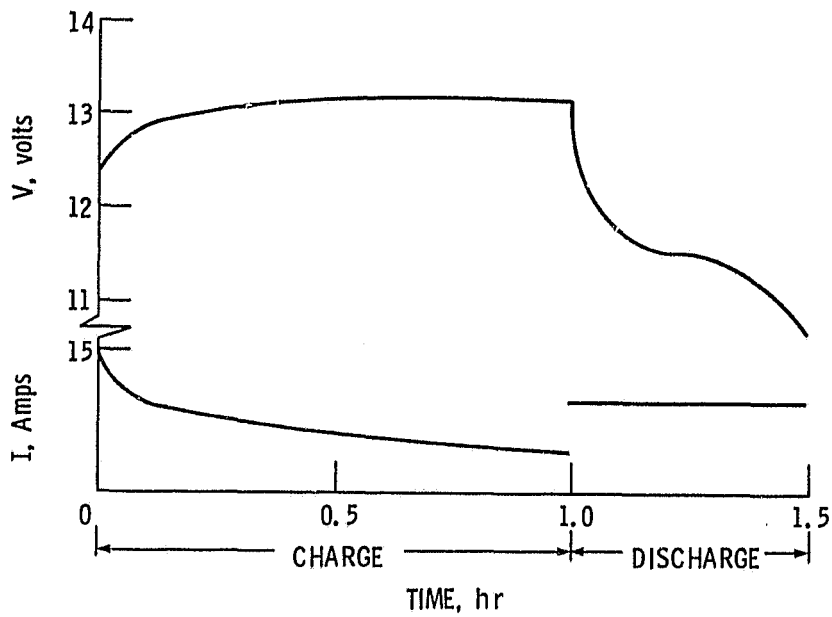


Figure 8. - Battery voltage and current for LEO cycle employing constant voltage charging.